

CONJUGATE HEAT TRANSFER AND FLOW DISTRIBUTION IN AN ASSEMBLY OF  
 MANIFOLDED FINNED TUBES

G. F. Jones  
 Geological Engineering  
 Los Alamos National Laboratory  
 Los Alamos, New Mexico

N. Lior  
 Department of Mechanical Engineering and Applied Mechanics  
 University of Pennsylvania  
 Philadelphia, Pennsylvania

ABSTRACT

Conjugate steady-state heat transfer and fluid flow (including buoyancy) in a vertical, externally irradiated assembly of manifolded finned tubes is analyzed from fundamental principles. The assembly consists of two horizontal circular manifolds interconnected by a number of plane-finned circular tubes. The problem has application to several types of heat exchangers including flat-plate solar collectors and plate heat exchangers. Buoyancy was found to tend to correct some of the flow maldistribution that would have occurred if the assembly was isothermal, by increasing the flow rate in the most flow-starved (and thus warmest) tubes. Results showing the influence of the main system parameters on heat exchanger flow distribution, thermal performance, and pressure drop are presented. For example, for an assembly that is characteristic of a flat-plate solar collector, at least one tube was found to receive a minimum of 15 percent less flow than average when the tubes were isothermal.

NOMENCLATURE (for major symbols and those not defined in text)

B dimensionless radiosity (scaled by  $\sigma T_1^4$ )  
 d inside diameter  
 g acceleration of gravity  
 Gr\* modified Grashof number for fluid,  
 $gBr^4 (T_{nb} + T_{df}) / (k_c v^2)$   
 h heat transfer coefficient  
 h length of tubes  
 $I^e$  dimensionless radiant flux from high temperature source ( $T/\sigma T_1^4$ )  
 k thermal conductivity based on  $T_1$   
 $\dot{m}$  mass flow rate  
 Nu local Nusselt number ( $h d_t / k_c$ )  
 n number of tubes in assembly  
 $P_c$  dimensionless fluid pressure ( $\bar{p}_c / \rho_1 \bar{v}_1^2$ )  
 $P'$  dimensionless pressure in manifold branch region ( $\bar{P}' / \rho_1 \bar{v}_1^2$ )  
 $P''$  dimensionless pressure in manifold non-branch region ( $\bar{P}'' / \rho_1 \bar{v}_1^2$ )

$P^*$  dimensionless pressure in tubes ( $\bar{P}^* / \rho_1 \bar{v}_1^2$ )  
 $\Delta P_{mb}$  dimensionless pressure drop from friction and inertia caused by buoyancy ( $\Delta \bar{P}_{mb} / \rho_1 \bar{v}_1^2$ )  
 $\Delta P_{hb}$  dimensionless hydrostatic pressure change from buoyancy ( $\Delta P_{hb} / \rho_1 \bar{v}_1^2$ )  
 Pr Prandtl number of fluid  
 r dimensional radial coordinate in tubes ( $\bar{r} / r_t$ )  
 $r_t$  tube radius  
 $R^l$   $\sigma T_1^3 \epsilon^l s^2 / [k_f t_f (1 - \epsilon^l)]$   
 $R^h$   $\sigma T_1^3 \epsilon^h s^2 / [k_f t_f (1 - \epsilon^h)]$   
 s fin half width  
 t thickness  
 T dimensionless temperature ( $\bar{T} / T_1$ )  
 u dimensionless tube local axial velocity [ $\bar{u} / (v / r_t)$ ]  
 U dimensionless tube mean velocity ( $\bar{U} / \bar{v}_1$ )  
 v dimensionless tube local radial velocity [ $\bar{v} / (v / r_t)$ ]  
 V dimensionless manifold mean velocity ( $\bar{V} / \bar{v}_1$ )  
 W length of manifolds  
 x local fin coordinate in fin transverse direction (see Fig. 3)  
 X global coordinate in direction of inlet manifold flow (see Fig. 2)  
 z dimensionless axial coordinate in tubes ( $\bar{z} / r_t$ )

Greek Symbols

$\delta$  fin-tube bond thickness  
 $\epsilon$  emissivity  
 $\eta$  dimensionless transverse coordinate in fin,  $(x - r_t) / s$   
 $\theta$  angular position for tube  
 u  $t_f / 2r_t$   
 $\nu$  kinematic viscosity (evaluated at  $T_1$ )  
 $\xi$  dimensionless axial coordinate ( $\bar{z} / h_e$ )  
 $\rho$  fluid density  
 $\sigma$  Stephan-Boltzmann constant  
 $\Phi$  dimensionless perturbed temperature for finned tube,  $(T - T_1) / T_1$   
 $\Psi$  dimensionless temperature,  $(T - T_1) / [(T_{df} + T_{nb}) r_t / k_c]$

Subscripts

|    |                           |
|----|---------------------------|
| a  | convective (ambient) sink |
| b  | bulk fluid                |
| c  | fluid                     |
| df | diffuse                   |
| f  | fin                       |
| h  | hydrostatic               |
| i  | inlet manifold            |
| m  | due to fluid motion       |
| nb | normal beam               |
| o  | outlet manifold           |
| s  | radiation sink            |
| t  | tube                      |
| T  | total                     |

Superscripts

|    |   |
|----|---|
| -- | dimensional pressure, velocity, and temperature |
| h  | high temperature source                         |
| l  | low temperature source                          |
| f  | fin   |
|    | ) on symbol {                                   |
| t  | tube  |

**INTRODUCTION**

We consider the problem of conjugate, steady-state heat transfer and fluid flow in a vertical, externally irradiated assembly of manifolded finned tubes as shown in Fig. 1. The assembly consists of two horizontal

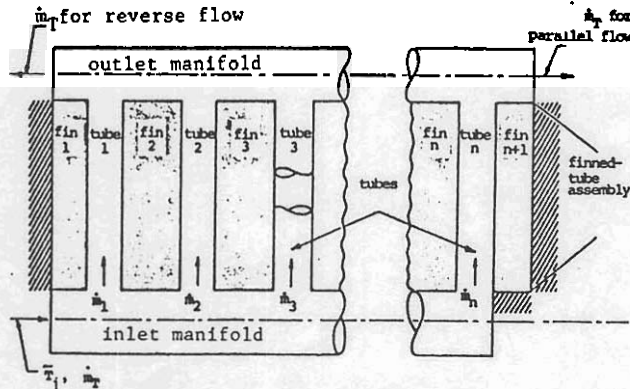


Fig. 1. Assembly of manifold finned tubes

circular manifolds interconnected by a number of plane-finned circular tubes. A fluid is pumped into one end of the lower manifold where it is distributed through the tubes, becomes heated, and then combined in the upper manifold. The fluid departs the assembly in either the same direction as the inlet flow (parallel flow configuration) or in the opposite direction (reverse flow configuration). This problem has application to several types of plate heat exchangers including flat plate solar collectors and plate heat exchangers where the inter-plate heat-transfer rate may be approximated as spatially constant.

In contrast to some of the previous manifold flow studies [cf. Bajura and Jones (1976), Bassiouni and Martin (1984a, 1984b)] the authors and their co-workers [Jones and Lior (1978), Menuchin et al. (1981)] and Hoffman and Flannery (1985) have included both inertial and frictional effects in the manifolds. Here, flow branching occurs at discrete locations along the manifolds with only frictional pressure loss in the non-branch regions. This formulation results in a system of nonlinear algebraic equations that must be

solved numerically. The advantage of this formulation is that it spans the entire range of manifold designs from inertially to frictionally dominant at the expense of increased difficulty of solution. Results for isothermal assemblies show that flow distribution becomes more uniform with decreased number of tubes (for a fixed manifold length), decreased ratio of tube diameter to manifold diameter, and with increased tube height-to-diameter ratio. Also, flow becomes uniformly distributed as the pressure drop in the tubes becomes the dominant one in the assembly.

In contrast to isothermal manifold systems, the interaction between manifold flow distribution and heat transfer to the fluid has received little attention because of its inherent complexity [Chiou (1982), Window and Harding (1983)]. The effect of a prescribed flow distribution pattern on thermal performance of flat plate collectors was shown to degrade efficiency by 2-20% with realistic collector fluid-flow distributions.

**ANALYSIS**

Manifold hydrodynamics. We formulate the manifold hydrodynamics part of the present conjugate problem assuming discrete flow branching in the manifolds. The geometry and definitions of the variables used in this formulation are given in Fig. 2. The manifold assembly

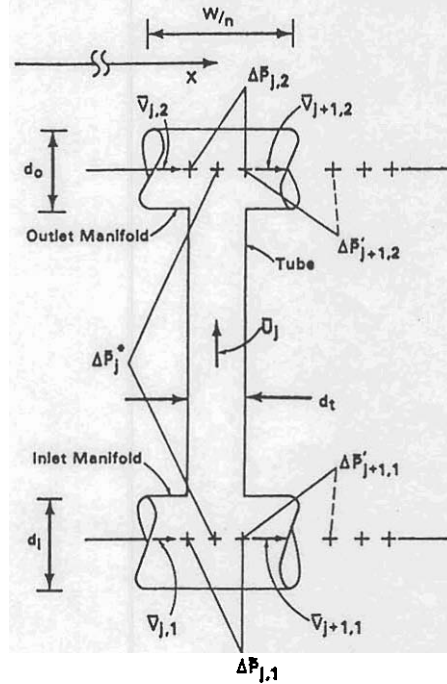


Fig. 2. Manifold geometry for j-th section

is divided into n increments, where n is the number of tubes, and manifold and tube velocities and pressure changes are identified with each increment. Specifically,  $\Delta P_{j,k}^*$ ,  $\Delta P_{j,k}'$ , and  $\Delta P_j^*$  refer to the pressure changes arising from inertial and frictional effects in the branch region for the jth increment and the kth manifold (k-1 for inlet manifold, 2 for outlet manifold), frictional effects in the non-branch region for the jth increment and the kth manifold, and frictional effects for the jth tube respectively. Manifold and tube velocities are  $V_{j,k}$  and  $U_j$ . Referring to Fig. 2, flow to the right and upwards is taken as positive

for the parallel flow configuration, and outlet-manifold flow to the left is taken as positive for the reverse flow case.

The fluid dynamics of manifold flow are described by Keller (1949), McNown (1954), Acrivos et al. (1959), Bajura (1971), and Bajura and Jones (1976). Here the dimensionless form of the momentum and mass conservation equations for a branch in the inlet manifold are

$$\Delta P_{j,1} = \beta_{j+1,1} V_{j+1,1}^2 - \beta_{j,1} V_{j,1}^2 + \gamma_{j,1} U_j V_{j,1} (d_t/d_i)^2, \quad 1 < j < n \quad (1a)$$

and

$$0 = V_{j+1,1} - V_{j,1} + U_j (d_t/d_i)^2, \quad 1 < j < n \quad (1b)$$

respectively, where  $\Delta P_{j,1} = P_{j,1} - P_{j+1,1}$ . The third term on the right hand side of Eq. (1a) corrects this pressure increase to account for loss of momentum from the manifold stream by the branching manifold flow.

$\gamma_{j,1}$  is the ratio of the velocity in the direction of inlet-manifold flow at the entrance to the tube mouth, to the branch inlet velocity  $V_{j,1}$ ; and is termed a "static pressure regain coefficient." It is determined empirically, and is a weak function of branch and manifold geometry, and branch-flow ratios as discussed below. A value of 1 for  $\gamma_{j,1}$  indicates a maximal loss of momentum in manifold flow, whereas a value of zero corresponds to no loss of momentum to the branching flow and the largest static pressure regain as seen from Eq. (1a). The terms  $\beta_{j,k}$  are dimensionless, momentum correction factors that convert the momentum flux based on mean velocity to that actually possessed by the flow for a prescribed flow regime. They are usually fixed at unity for the experiments performed to obtain the  $\gamma$  coefficients.

A modified Bernoulli equation is written in dimensionless form to express pressure loss in a non-branch region

$$\Delta P'_{j,1} = f_{m,j,1} [W/(n d_t) - 1] (d_t/d_i)^2 V_{j,1}^2/2, \quad 2 < j < n. \quad (2)$$

For parallel flow, the equations corresponding to Eqs. (1) and (2) for the outlet manifold are

$$\Delta P_{j,2} = \beta_{j+1,2} V_{j+1,2}^2 - \beta_{j,2} V_{j,2}^2 - \gamma_{j,2} U_j V_{j+1,2} (d_t/d_o)^2, \quad 1 < j < n. \quad (3a)$$

$$0 = V_{j+1,2} - V_{j,2} + U_j (d_t/d_o)^2, \quad 1 < j < n \quad (3b)$$

$$\Delta P'_{j,2} = f_{m,j,2} [W/(n d_t) - 1] (d_t/d_o)^2 V_{j,2}^2/2, \quad 2 < j < n. \quad (4)$$

In Eq. (3a),  $\gamma_{j,2}$  is a dimensionless, empirically determined "static pressure decrease coefficient" and accounts for the transport of momentum in the direction of outlet manifold flow from the combining tube stream, and momentum loss from turbulent mixing of the two streams.

A modified Bernoulli equation in dimensionless form for the tube flow is

$$\Delta P_j^* = (1 + c_c + c_d + f_{r,j} h_e/d_t) U_j^2/2 + \Delta P_{mb,j} + \Delta P_{hb,j}, \quad 1 < j < n \quad (5)$$

where  $c_c$  and  $c_d$  are empirically determined mechanical-

energy loss coefficients that account for flow turning in outlet and inlet manifold branches, and  $f_{r,j}$  is an axially averaged friction factor for isothermal, developing flow in the tubes.  $\Delta P_{mb,j}$  and  $\Delta P_{hb,j}$  account for pressure changes arising from buoyancy in the tubes attributed to fluid motion (inertial and frictional pressure drop), and the buoyant part of hydrostatic pressure change, respectively. For an isothermal assembly,  $\Delta P_{mb,j}$  and  $\Delta P_{hb,j}$  are both zero. These terms are discussed in more detail further below.

Since the mean pressure at any location in the assembly is single-valued, the net pressure change around any closed loop is zero. The loop equation for parallel flow is

$$0 = \Delta P_j^* - \Delta P_{j+1}^* + \Delta P'_{j+1,2} - \Delta P'_{j+1,1} + (\Delta P_{j,2} + \Delta P_{j+1,2} - \Delta P_{j,1} - \Delta P_{j+1,1})/2 \quad 1 < j < n-1 \quad (6)$$

Equations (1-6) are a system of  $(10n-3)$  simultaneous algebraic equations for  $10n$  pressure and velocity variables. The boundary conditions are

$$V_{1,1} = 1, \quad V_{n+1,1} = 0, \quad \text{and}$$

$$V_{1,2} = 0 \text{ (parallel flow) or } V_{n+1,2} = 0 \text{ (reverse flow).}$$

Values for the flow coefficients  $\gamma_{j,1}$ ,  $\gamma_{j,2}$ ,  $c_d$ , and  $c_c$  have been empirically determined by McNown (1954) and Acrivos et al. (1959).

**Heat transfer in the finned tubes.** The finned tube geometry is shown in Fig. 3. To be consistent

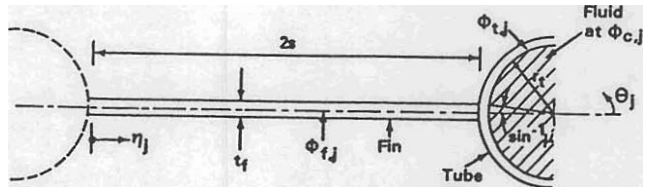


Fig. 3. Finned-tube geometry for  $j$ -th section

with the manifold-hydrodynamics formulation, the assembly is divided into  $n$  increments corresponding to the number of tubes; each increment consisting of a tube and the fin to its left. High temperature-source diffuse and normal-beam radiation from  $T_{df}$  and  $T_{nb}$  and low temperature-source radiation from temperature  $T_a$  are incident on the front surface of the assembly. Conduction and radiation heat transfer occur from the  $j$ th and  $(j+1)$ st fins to the  $j$ th tube, and the tube is irradiated directly. The assembly loses heat by convection through a constant heat transfer coefficient ( $h_c$ ) to temperature  $T_a$ , by radiation outward from the front surface, and by combined forced/natural convection through variable heat transfer coefficient ( $h_j$ ) to the tube fluid at bulk temperature  $T_b$ . For the analysis that follows, we assume that the thickness of the bond between the fins and tubes and heat loss through the back of the assembly are negligibly small, although they may be included without much difficulty.

In contrast with previous formulations of heat transfer in collectors, in particular the Hottel-Whillier-Bliss (HWB) model (Hottel and Woertz 1942, Whillier 1953, Bliss 1959, Chiou 1959) which neglect fin/tube radiant interaction, we include radiant interaction among semigray (Lieblein 1959, Plamondon and Landram 1966), diffuse fin/tube surfaces in the present formulation.

Assuming that  $h_e/s \gg 1$  so that fin conduction may be approximated as one-dimensional, the steady constant-property energy equation in dimensionless form for the  $j$ th fin is

$$d^2 \phi_{f,j} / dn^2 - \lambda^2 (\phi_{f,j} + P_f) + R^1 B_{f,j}^1(n, \xi^f) + R^h B_{f,j}^h(n) = 0, \quad 1 < j < n+1 \quad (7a)$$

where  $B_{f,j}^1$  and  $B_{f,j}^h$  are dimensionless low and high temperature-source radiositivities for a differential element of fin area located at  $(n, \xi^f)$ ; the former composed of emitted plus reflected incident energy from low-temperature sources, and the latter of only reflected incident energy from the high-temperature source.  $\lambda^2$  is the ratio of radiative plus convective conductance from the front of the fin, to the conduction conductance in the fin.  $P_f$  is a constant dimensionless fin temperature resulting from convection and radiation from the fin surface.  $R^1$  and  $R^h$  are constants.

$$P_f = [h_a(1-T_a) + \sigma \epsilon^1 \bar{T}_i^3 / (1-\epsilon^1)] s^2 / (k_f t_f \lambda^2) \quad (7b)$$

$$\lambda^2 = [h_a + 4 \epsilon^1 \sigma \bar{T}_i^3 / (1-\epsilon^1)] s^2 / (k_f t_f)$$

Because temperature variations in the fin are expected to be smaller than the absolute temperature  $\bar{T}_i$ , we use a dimensionless perturbed temperature  $\phi_{f,j}$  in Eq. (7a) defined as  $(T_{f,j} - \bar{T}_i) / \bar{T}_i$ . This approach simplifies the problem since the nonlinear emission term may then be linearized by using a truncated binomial expansion (Eno, 1976) where,

$$(\bar{T}_{f,j} / \bar{T}_i)^4 = (1 + \phi_{f,j})^4 = 1 + 4\phi_{f,j} + 6(\phi_{f,j})^2 + \dots, \quad \phi_{f,j} < 1. \quad (8)$$

If only the first two terms in the series are retained for use in the energy balance, errors in temperature of less than a few percent are expected since typical values of  $\phi_{f,j}$  are 0.1 or smaller.

The expressions for fin radiosity are

$$B_{f,j}^1(n, \xi^f) = \epsilon^1 [1 + 4 \phi_{f,j}(n, \xi^f)] + \alpha_{j-1}(n) (1 - \epsilon^1) \left\{ \Gamma_{j-1} \int_{\sin^{-1}u}^{\alpha_{j-1}(n)} B_{t,j-1}^1(\theta, \xi^f) K(\theta_{j-1}, \eta_j) d\theta + \Gamma_j \int_{\alpha_j(n)}^{\pi - \sin^{-1}u} B_{t,j}^1(\theta, \xi^f) K(\theta_j, \eta_j) d\theta \right\} + \Gamma_s^4 F_{(f-s),j}(n), \quad 1 < j < n+1. \quad (9a)$$

$$B_{f,j}^h(n) = (1 - \epsilon^h) \left\{ \Gamma_{j-1} \int_{\sin^{-1}u}^{\alpha_{j-1}(n)} B_{t,j-1}^h(\theta) K(\theta_{j-1}, \eta_j) d\theta + \Gamma_j \int_{\alpha_j(n)}^{\pi - \sin^{-1}u} B_{t,j}^h(\theta) K(\theta_j, \eta_j) d\theta \right\} + I_{df} F_{(f-s),j}(n) + I_{nb}, \quad 1 < j < n+1 \quad (9b)$$

In Eq. (9), it was assumed that  $h_e/s \ll 1$  as before, so that the two manifold pipes do not participate in the radiation processes. The finned tubes are diffuse reflectors of low temperature source radiation to be consistent with the high-temperature source radiation.  $\alpha_{j-1}$  and  $\alpha_j$  are the angles defining the upper and lower limits of visibility for the tube when viewing a fin. The kernels of the integral equations,  $K$ , are from diffuse configuration factors between fin differential-area elements and infinitely-long, differentially-wide elements of tube area (Sotos and Stockman, 1964). It has been demonstrated by Sparrow and Krowech (1977) that most of the heat transfer between fin and tube elemental areas occurs for elements having the same axial coordinates. Thus, radiant exchange between a fin element at  $\xi^f$ , and two parallel tubes, can be approximated as if the tubes are infinite in length and axially isothermal, at the temperature corresponding to that location.

$F_{(f-s)}$  are diffuse configuration factors for a differential element of fin area viewing the isothermal surface in front of the assembly. The terms  $\Gamma$  in Eq. (9) are one or zero depending on the value of  $j$ ; for  $j=1$ ,  $\Gamma_{j-1} = 0$ , for  $j=n$ ,  $\Gamma_j = 0$ , and  $\Gamma_j = 1$  otherwise.

For thin-walled tubes, results from an order-of-magnitude analysis show that axial conduction and radial temperature gradients in the tube wall are negligibly small. In addition, the circumferential variation of tube-wall temperature and heat flux is also shown to be negligible if the thermal conductivity of the tube is large, and the tube-wall energy balance is thus formulated as quasi-one dimensional, which, in dimensionless form, becomes

$$\phi_{t,j}(\xi^t) - P_{t,j}(\xi^t) - \lambda_{t,j}(\xi^t) \phi_{b,j}(\xi^t) = 0, \quad 1 < j < n. \quad (10)$$

where  $\phi_{t,j}$  and  $\phi_{b,j}$  are dimensionless perturbed tube and bulk fluid temperatures defined in the same manner as fin temperature, and  $P_{t,j}$  and  $\lambda_{t,j}$  depend on flow and heat transfer in and outside of a tube.

$$\omega_{t,j} P_{t,j}(\xi^t) = (\sigma \bar{T}_i^3 r_t [ \int_{\sin^{-1}u}^{\pi - \sin^{-1}u} (\epsilon^1 B_{t,j}^1(\theta, \xi^t) / (1-\epsilon^1) + \epsilon^h B_{t,j}^h(\theta) / (1-\epsilon^h)) d\theta ] + \sigma \bar{T}_i^3 a_r \epsilon^1 / (1-\epsilon^1) + h_a a_r (1-T_a) s) / (k_f t_f) - \partial \phi_{f,j} / \partial \eta |_{\eta=2} + \partial \phi_{f,j+1} / \partial \eta |_{\eta=0}$$

$$\omega_{t,j} \lambda_{t,j}(\epsilon^t) = \pi k_c Nu_j(\epsilon^t) s / (k_f t_f) \quad (11b)$$

$$\omega_{t,j} = [4 \sigma \bar{T}_i^3 a_r \epsilon^1 / (1 - \epsilon^1) + \pi k_c Nu_j(\epsilon^t) + h_a a_r] s / (k_f t_f) \quad (11c)$$

where  $a_r = r_t(\pi - 2\sin^{-1}u)$  is the perimeter of the top side of a tube. In Eq. (10), the tube-wall temperature is a linear function of the bulk fluid temperature.  $\lambda_{t,j}$  is the ratio of the convective conductance between the tube wall and the fluid, to the sum of all conductances from the tube to the external radiative and convective sinks and to the fluid. The term  $P_{t,j}$  is a dimensionless stagnation temperature for the tube which occurs for  $Nu_j$  equal to zero (or no fluid flow).

Radiosity distributions for the tubes are written in the same way as for the fins in Eq. (9) but are not presented here for brevity. In this case, radiant contributions to a differential element of tube area are from the adjacent tube and fin that view it, and the radiant sink temperature or high temperature source as before.

The finned tubes are insulated along the outer edges. The remaining boundary condition is a matching of the fin and tube temperature where they are in contact. Thus, temperature continuity is satisfied across the fin and tube interface, and Eq. (11) satisfies continuity of heat flow there.

Fluid flow and heat transfer in a tube. The configuration considered is upward flow of a Boussinesq fluid in  $n$  externally vertical circular tubes of length  $h_e$  and radius  $r_t$ , which, equally spaced, connect an inlet manifold to an outlet manifold. The radial and axial direction and velocity components are denoted as  $(\bar{r}, \bar{z})$  and  $(\bar{v}, \bar{u})$ , respectively. The mean velocity at the inlet to each tube is  $\bar{U}_j$ , and the inlet temperature for all tubes is  $\bar{T}_i$ . We predict the pressure and temperature distribution for each tube and couple this information to the parts of the problem that treat finned-tube heat transfer and manifold hydrodynamics. In this way, mass, momentum, and energy conservation for the entire assembly are satisfied simultaneously. As an example of this coupling, heat transfer to a particular tube influences the tube friction factor which affects a change in the tube fluid flow rate and, in turn, alters the rate of heat transfer from the original value.

The topic of developing, buoyancy-assisted combined convection in a vertical tube has received considerable attention in the past. The studies performed considered either constant temperature (Zeldin and Schmidt 1972, Marnar and McMillan 1970, Lawrence and Chato, 1966), or constant heat flux tube walls (Zeldin and Schmidt 1972, Lawrence and Chato 1966). Because the more realistic conjugate problem is being solved in this study, neither of these conditions may be imposed; rather simultaneous solution of the problem coupling all subsystems is executed. As is often the case for flow in compact and plate heat exchangers having smooth and small flow passages, and relatively low velocity, it is assumed that the flow is laminar. The inlet velocity to each tube is taken to be uniform. After an entry length (of about 10 tube diameters for the cases considered here) the radial pressure gradient is negligible. In the usual way, the axial pressure gradient ( $d\bar{p}/d\bar{z}$ ) is expressed as the sum of two independent pressure gradients: one attributed to fluid motion and the other arising from hydrostatics:

$$d\bar{p}_c/d\bar{z} = d\bar{p}_m/d\bar{z} + d\bar{p}_h/d\bar{z} \quad (12)$$

where  $d\bar{p}_h/d\bar{z} = -\rho_i g$ , and is referenced to tube-wall temperature. With  $\rho_c = \rho_i [1 + \beta(\bar{T}_i - \bar{T}_c)]$ , where  $\beta$  is the coefficient of thermal expansion.

$$d\bar{p}_h/d\bar{z} = -\rho_i g + \rho_i g \beta (\bar{T}_t - \bar{T}_i) \quad (13)$$

Since convective acceleration is small for this case, the axial component of the momentum equation using Eqs. (12) and (13) is

$$d\bar{p}_m/d\bar{z} = -\rho_i g \beta (\bar{T}_t - \bar{T}_c) + [\text{viscous terms}]. \quad (14)$$

In Eq. (14), the temperature difference term is positive and the viscous terms are negative, so we see that the effect of buoyancy on the flow is to increase the axial pressure gradient  $d\bar{p}_m/d\bar{z}$  relative to that in the isothermal case.

The total pressure gradient is now written from Eqs. (12)-(14)

$$d\bar{p}_c/d\bar{z} = -\rho_i g \beta (\bar{T}_t - \bar{T}_c) + [\text{viscous terms}] + \rho_i g \beta (\bar{T}_t - \bar{T}_i) - \rho_i g. \quad (15)$$

The first two terms on the right-hand side of Eq. (15) represent the contribution from fluid motion ( $d\bar{p}_m/d\bar{z}$ ), and the third and fourth terms are the buoyant and isothermal contributions from hydrostatics respectively. The fourth term is 2-3 orders of magnitude smaller than the rest and for this reason it will be neglected. The first and third terms in Eq. (15) combine to form a single positive-valued buoyancy term (because  $\bar{T}_t > \bar{T}_i$ ) and since the viscous terms are negative, the overall effect of buoyancy on forced upward flow in an isolated, externally heated tube is to reduce the total pressure gradient relative to the isothermal case. This is equivalent to a reduction in tube friction factor when compared with that for isothermal flow. It is this effect that causes an increased tube flow rate with tube-wall temperature as cited in the example above. Compared with isothermal conditions, the partially flow-starved (and thus warmest) tubes in the assembly exhibit a reduced flow resistance compared with cooler tubes and, hence, an increase in fluid flow rate when buoyancy effects exist.

Past numerical studies of assisting combined convection in an inclined tube (Cheng and Hong 1972a, 1972b) have shown that local friction factors and Nusselt numbers are independent of Prandtl number and increase monotonically with angle of inclination from the horizontal, till a vertical orientation is reached. Increased local heat transfer in the tubes increases performance of the assembly directly, and also indirectly through more uniform flow distribution as discussed above. It follows then that solutions of the present problem, which treats vertical tubes, represent an upper bound on improvement in thermal performance over the isothermal case.

Based on the preceding developments, the following is to be used with Eq. (5)

$$\Delta\bar{p}_{hb} = (2 \int_0^{h_e} \int_0^{r_t} (\partial\bar{p}_h/\partial\bar{z}) \bar{r} d\bar{r} d\bar{z}) / r_t^2 + \rho_i g h_e. \quad (16a)$$

$$\Delta \bar{P}_{mb} = -2 \int_0^h \int_0^{r_t} [(\partial \bar{p}_m / \partial z)_{\text{buo.}} - (\partial \bar{p}_m / \partial z)_{\text{iso.}}] r dr dz / r_t^2. \quad (16b)$$

where the first term in parenthesis in Eq. (16b) accounts for the actual pressure gradient for a tube having an externally heated wall, and the second one is the pressure gradient occurring for the same hydrodynamic conditions if the flow is isothermal.

For the case where the Peclet number for tube flow is greater than 100, so that axial momentum and heat transport are neglected, the equations governing mass, momentum, and energy conservation in dimensionless form for the flow in each tube are

$$\partial(rv)/r\partial r + \partial u/\partial z = 0. \quad (17a)$$

$$v\partial v/\partial r + u\partial v/\partial z = -\partial p_m/\partial r + \partial(r\partial v/\partial r)/r\partial r - v/r^2. \quad (17b)$$

$$v\partial u/\partial r + u\partial u/\partial z = -\partial p_m/\partial z + \partial(r\partial u/\partial r)/r\partial r - Gr^*(\psi_t - \psi_c). \quad (17c)$$

$$v\partial \psi_c/\partial r + u\partial \psi_c/\partial z = [\partial(r\partial \psi_c/\partial r)/r\partial r]/Pr. \quad (17d)$$

In Eqs. (17a)-(17d), the velocity components, pressure, and coordinates are scaled with  $v/r_t$ ,  $p_i(v/r_t)^2$ , and  $r_t$ , respectively. The boundary conditions are

$$v(r=0, z) = v(r=1, z) = u(r=1, z) = \partial u/\partial r (r=0, z) = 0. \quad (17e)$$

$$p_m(r, z=0) = \partial p_m/\partial r (r=0, z) = \partial \psi_c/\partial r (r=0, z) = 0. \quad (17f)$$

$$u(r, z=0) = Re/2 = \bar{U}d_t/2\nu. \quad \psi_c(r=1, z) = \psi_c(z). \quad (17g)$$

where  $Pr$  is the Prandtl number,  $Re$  is the tube Reynolds number, and  $Gr^*$  is a modified Grashof number.

This part of the conjugate problem is coupled to the remaining two parts through the buoyancy term in Eq. (17c) where the tube-wall temperature affects the velocity and temperature fields for the fluid in each tube, and through the boundary condition at the tube entrance where the tube Reynolds numbers result from manifold hydrodynamics.

#### METHOD OF SOLUTION

The equations that govern the temperature, radiosity, pressure, and velocity distributions for the conjugate problem are simultaneous nonlinear partial differential equations [for fluid flow and heat transfer in a tube, Eq. (17)], simultaneous linear ordinary integro-differential equations [for heat transfer in the finned tubes, Eq. (7)-(11)], and simultaneous nonlinear algebraic equations [for manifold hydrodynamics, Eq. (1)-(6)]. A system of simultaneous linear integral equations [for the high temperature-source radiosity, Eq. (9b)] needs to be solved initially to produce  $B^h$  distributions for the finned tube. The problems associated with the first three equation systems are viewed as components of the conjugate problem and are referred to as "sub-problems." The solution to the conjugate problem is obtained by solving one subproblem after another in sequence, and re-solving them until convergence is reached. The solution to the conjugate problem is hence refined with each cycle of this "overall iterative procedure" because any one subproblem is solved subject to boundary conditions that correspond to the most recent solutions for the remaining two.

A schematic block diagram of this procedure is

presented in Fig. 4. Each step in the procedure is

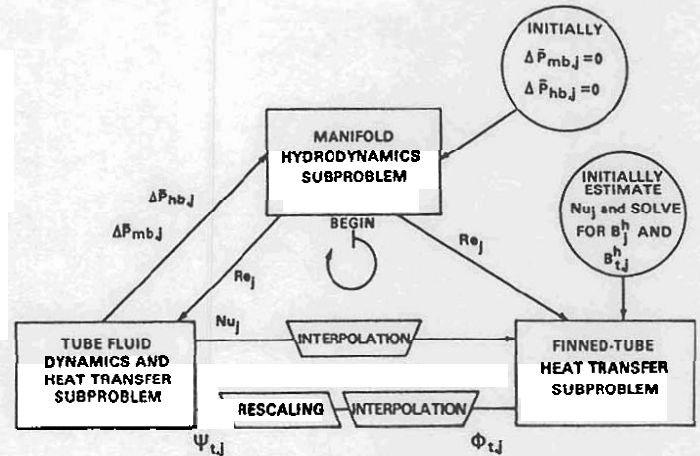


Fig. 4. Block diagram for solution of conjugated problem indicating coupling among subproblems.

described briefly below. Isothermal conditions are initially assumed. (1) The first step is to solve for high temperature-source radiosity distributions which remain unchanged throughout the procedure. (2) Solve the equations for manifold hydrodynamics to obtain flow distribution and calculate Reynolds numbers for each tube. (3) For the first cycle of the procedure only, estimate local Nusselt numbers from a suitable correlation (Churchill and Ozoe 1973) using Reynolds numbers from step 2. (4) Calculate low temperature-source radiosity and temperature distributions for the fins and tubes from the equations for finned-tube heat transfer and most recently estimated Nusselt numbers; from a macroscopic energy balance on the flow in each tube, re-estimate the bulk fluid temperature. (5) Solve for the fluid temperature, pressure, and velocity distributions in each tube subject to most recent tube Reynolds numbers and tube-wall temperatures; re-estimate Nusselt number distributions for each tube. (6) From the most recent tube-wall temperatures, evaluate  $\Delta P_{bh}$  for each tube from Eqs. (13) and (16a); from a correlation for hydrodynamically developing isothermal flow (Shah 1978), and pressure distributions from step 5, evaluate  $\Delta P_{mb}$  for each tube from Eq. (16b), and (7) Repeat steps 2 through 6 until convergence occurs.

Vehicles for information transfer among the subproblems, as seen in Fig. 4 and described above, are summarized in the following table.

Vehicles for Information Transfer Among the Subproblems

|                           | Manifold Hydrodynamics | Finned-tube Heat Transfer | Fluid Dynamics and Heat Transfer in a Tube       |
|---------------------------|------------------------|---------------------------|--|
| Manifold Hydrodynamics    | --                     | $Re_j$                    | $Re_j$<br>$\Delta P_{mb,j}$<br>$\Delta P_{hb,j}$ |
| Finned-tube Heat Transfer |                        | --                        | $\phi_{t,j}$<br>(or $\psi_{t,j}$ )<br>$Nu_j$     |

Local Nusselt numbers have been used in the past as vehicles for information transfer between parts of a conjugate problem by Sparrow and Faghri (1980), and they work well.

The manifold-hydrodynamics subproblem was solved by the Newton-Raphson method which used Choleski decomposition (for parallel flow cases) or Gauss-Jordan reduction (for reverse flow). Convergence was achieved when all equations were satisfied to within a dimensionless velocity and pressure change of  $10^{-4}$ . The equations for finned-tube heat transfer were solved by finite differences using 11 nodes for the fin in the transverse direction and for the tube in the circumferential direction. Five-point backward or forward differences were used for the temperature gradients in Eq. (11a). The kernel functions and configuration factors in the radiosity integral equations were evaluated for all fin- and tube-node combinations. Because of the sensitivity of the kernels and configuration factors to slight changes in coordinate values in the neighborhood of the fin/tube interfaces, the nodes nearest to the interfaces were sub-divided into 10 finer nodes and the kernels and configuration factors were calculated for these and then averaged. Integral equations were approximated by a sixth-order Simpson's rule with fourth-order end corrections. The system of linear algebraic equations was solved by Gauss-Seidel iteration using a relative convergence criterion of  $10^{-4}$ . The radiosity integral equations for the high temperature-source were approximated in the same way and solved by iteration where convergence was achieved when all equations were satisfied to within  $10^{-8}$  dimensionless radiosity units.

The equations for fluid flow and heat transfer in the tubes were solved by finite differences using a fine axial-direction mesh in the region near the tube mouth and a coarser mesh downstream from this. Typically, 41 radial and first-region axial nodes were used with 31 second-region axial nodes. Upwind differences were used for axial convection and central differences for the diffusion terms. The equations were solved implicitly by marching in the downstream direction, solving for velocity, pressure, and temperature at all radial nodes for each step of the march. A sparse-coefficient, linear algebraic equation solver (Gupta and Tanji 1977), which employs matrix decomposition, was used to solve the system of linear algebraic equations at each axial location.

Only about three of four cycles were required to converge the "overall iterative procedure", described in Fig. 4, except for several cases with large tube diameters which required six or seven cycles because of

the stronger effects from buoyancy. Typical running time on an IBM 4341 computer was about 1250 seconds for an assembly of four tubes, which converged in four cycles.

RESULTS AND DISCUSSION

Because the principal focus is on flow distribution, tube diameter and tube length were selected as primary parameters since these not only affect flow distribution for an isothermal assembly but also influence heat transfer to the tube fluid (through  $Gr^*$  and flow development considerations). The analysis was also performed for parallel and reverse flow configurations. It has been shown by Jones and Lior (1978) that nearly uniform flow conditions exist for  $d_t/d_i$  ( $=d_t/d_o$ ) of 0.25 and smaller, and so we take this as the lower bound for  $d_t$ . A reasonable upper bound was assumed to be  $d_t/d_i = 0.75$ . The specific example for which this analysis was used concerned flat plate solar collectors which typically have manifold diameters of about 1.27 cm and tube lengths of 1 to 2 m. To investigate the effect of tube length on flow distribution and performance, we choose two values for tube length: 0.61 m ("short assembly"), and 1.83 m ("long assembly"). The remaining variables are fixed at the values as shown below.

|  |                                 |                                 |
|--|---------------------------------|---------------------------------|
| $\dot{m}_T = 0.015$ kg/s                             | $\bar{T}_j = 300$ K             | $\bar{T}_a = \bar{T}_s = 289$ K |
| $t_f = 0.76$ mm                                      | $s = 5.98$ cm                   | $k_f = 173.1$ W/m K             |
| $\bar{T}_{df} = \bar{T}_{nb} = 315$ W/m <sup>2</sup> | $h_a = 2.84$ W/m <sup>2</sup> K | $n = 4$                         |
| $\epsilon^l = 0.2$                                   | $\epsilon^h = 0.9$              | fluid: water                    |

Four tubes (risers) were chosen for computational convenience. The expected results for assemblies having more than four tubes are briefly discussed below.

To address the effect of buoyancy on flow distribution and assembly performance, two limiting cases were considered: one with and one without buoyancy effects. The solution of the conjugate problem is thus obtained for 24 different combinations of variables: three diameter ratios for short and long assemblies for both upper- and lower-bound cases, and for parallel and reverse flow.

The influence of buoyancy on flow distribution, overall pressure drop, and thermal performance for all 24 combinations is presented in Fig. 5 where ratios of these quantities are plotted for the lower-(l) and upper-(u) bound cases against diameter ratio.  $\Delta P_T$  is the total dimensionless pressure drop for the assembly (scaled by  $\rho_i \bar{V}_{i,1}^2$ ) less ( $-\rho_j g h_e$ ) as discussed above. The thermal performance,  $E$ , is the ratio of the instantaneous heat transfer to the fluid, to the total irradiance on the surface of the assembly. The variable  $\kappa$  is a dimensionless flow maldistribution fraction defined as

$$\kappa = (\dot{m}_{max} - \dot{m}_{min}) / \dot{m}_i / n \quad (18)$$

where the denominator is the mass flow rate per tube for uniformly distributed flow.  $\kappa$  is the difference between the maximal and minimal dimensionless mass flow for the tubes.  $\kappa = 0$  indicates uniform flow distribution, whereas a nonzero value shows maldistributed tube flow; larger values indicating larger maldistribution.

Referring to Fig. 5, the results for  $d_t/d_i = 0.25$  (where the flow distribution is approximately uniform)

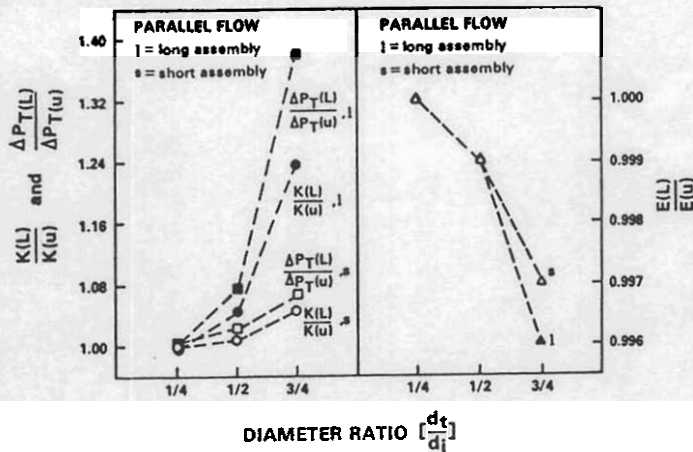


Fig. 5. Ratio of maldistribution fraction ( $\kappa$ ), overall dual-manifold system pressure drop ( $\Delta P_T$ ) and thermal efficiency ( $E$ ) for the ratio of lower- to the upper-bound cases for both assembly lengths and for parallel flow. Results for reverse flow are identical.

indicate practically no influence from buoyancy for all cases. This is because  $Gr^*$  is only 556 in contrast to a tube Peclet number of about 7200, so that heat transfer to the coolant is dominated by forced convection. The effect of natural convection is seen to increase with the diameter ratio. At  $d_2/d_1 = 0.75$  (where  $Gr^*$  is about 45,000), the overall pressure drop in the assembly decreases from the isothermal value by about 38 percent and the maldistribution fraction is reduced about 24 percent for the long assembly and for parallel and reverse flow. For the short assembly, buoyancy effects are weaker because of a smaller difference between the mean tube-wall and fluid temperatures and an overall lower temperature increase in the fluid. For all cases, we note a thermal performance increase of 0.4 percent or less (as measured from the lower-bound case) when buoyancy is included. In analyzing this result, we note that buoyancy which assists the flow in the tubes enhances performance directly by increasing the rate of heat transfer to the fluid (just as the pressure gradient  $dP/dz$  is increased), and indirectly by causing an adjustment of the tube flow toward uniformity. The first effect causes smaller temperature differences between the tube wall and the fluid resulting in cooler tube and fin temperatures and thus smaller heat losses. However, if the tube Peclet number is large, the coolant and tube-wall temperature rise is small so that a further slight decrease in tube-wall temperature caused by improved heat transfer between it and the fluid is negligible. The minimal Peclet number for the examples considered here is about 1600, large enough to explain the very small improvement due to buoyancy.

The second effect is explained with the help of Fig. 6 which shows dimensionless tube flow rates for each of the four tubes in the assembly for the short and long, and upper- and lower-bound cases. Also shown for reference is the uniform flow distribution assumed for a "base" case (b) which corresponds to the HWB model discussed above. Although the maldistribution fraction indicates a 24 percent change in going from the lower-bound to upper-bound cases for the long assembly, the actual change in flow distribution is not very large. In the first tube, the flow increases from 0.85 to 0.90, and in the last tube, the flow decreases

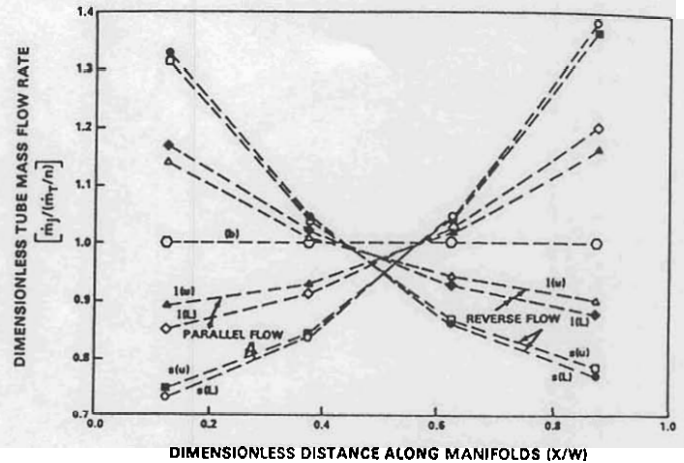


Fig. 6. Dimensionless mass flow rate among riser tubes for  $d_2/d_1 = 0.75$ , long, l, short, s, assemblies and upper- (u) and lower- (L) bound and base-model (b) cases.

to 1.16 from 1.20. Similar conclusions are drawn from the results for reverse flow. Fig. 6 also shows that the manifolds are inertially dominant; the last tube (nearest  $X=1$ ) having more than average flow, and the first tube less than average for parallel flow (and the opposite for reverse flow). This arises because of the relatively small tube spacing of about 11.1 cm so that frictional pressure losses in the non-branch regions are small when compared with inertial pressure changes in the branches.

Dimensionless fin temperatures are shown in Fig. 7

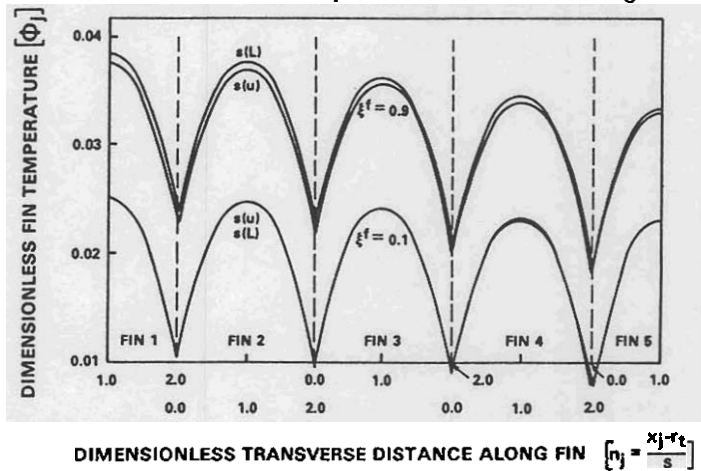


Fig. 7. Dimensionless fin temperature distribution ( $\phi_f$ ) for dimensionless axial locations ( $\bar{z}/h$ ) of 0.1 and 0.9 for  $d_2/d_1 = 0.75$ , short assembly and lower- (l) and upper- (u) bound cases.

for the short assembly and for the upper- and lower-bound, and base cases. The diameter ratio is 0.75 and temperatures are plotted for dimensionless axial locations of 0.1 and 0.9. The profiles indicate slightly cooler fin temperatures for the right side of the assembly than for the left because of the larger flow of fluid through tubes 3 and 4 compared with tubes 1 and 2. This difference is small, however, amounting to only 2-3 K. The reduction in fin temperature in

going from the lower- to upper-bound cases, is imperceptible for the axial location (along tube)  $z^*$  of 0.1 and is measurable but small for  $z^*$  of 0.9.

Developing axial velocity and temperature distributions for the flow in a single tube are presented in Fig. 8 for the upper-bound case of a 0.75

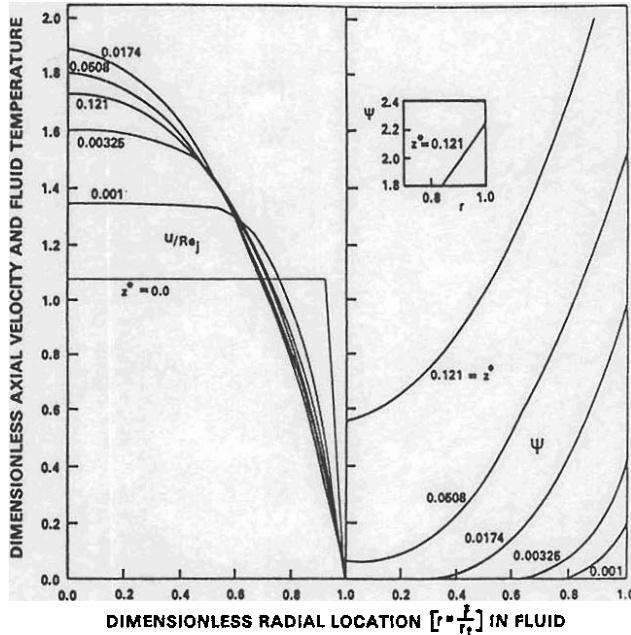


Fig. 8. Developing dimensionless axial velocity and temperature for tube-fluid, and for several  $z^*$  locations.  $Gr^* = 4.5 \times 10^4$  and  $Re = 538$ .

diameter ratio, long assembly. Here,  $Gr^*$  is 45,000 and the tube Reynolds number is 538. The profiles are shown for six dimensionless axial locations defined as  $z^* = [z/r_c, Pe]$ , where  $Pe = Re Pr$ ; the tube inlet, three intermediate  $z^*$  values,  $z^* = 0.0174$  corresponding to the location of maximal axial velocity at the tube centerline, and  $z^* = 0.121$  which is the tube outlet. Flow and thermal profile development proceed from the tube entrance up to  $z^* = 0.0174$  with the radial gradients of velocity and temperature decreasing with axial distance as usual. At this location, the thermal boundary layer progressed from the tube wall to about  $r = 0.3$  with buoyancy sufficiently strong to cause a reversal in the growth of velocity at the tube centerline. From  $z^*$  of 0.0174 to 0.0508, the velocity at this location decreases by about 5 percent and, through mass conservation, produces increased velocity gradients at the tube wall resulting in an increased axial pressure gradient. The radial temperature gradients also increase at the tube wall because of increased axial convective heat transfer there. At  $z^* = 0.0508$ , the thermal boundary layer has complete enveloped the flow field and at  $z^* = 0.121$ , the tube outlet is reached with the centerline velocity 9 percent lower than its value at  $z^* = 0.0174$  and about 15 percent lower than the isothermal asymptotic value of 2.0.

#### CONCLUSIONS

The complete formulation and solution of conjugate heat transfer and flow distribution in an assembly of manifolded finned tubes was carried out. The results obtained indicate that for tube-to-manifold diameter

ratios of 0.25 and smaller, tube flow is nearly uniformly distributed and there is negligible influence from buoyancy. As diameter ratio increases, flow maldistribution for an isothermal assembly also increases but is lessened somewhat when the assembly is externally heated and buoyancy in the tubes included. Pressure drop through the assembly decreases when the assembly is heated. For an assembly consisting of four tubes and a diameter ratio of 0.5, the effect of buoyancy is to reduce isothermal pressure drop and flow maldistribution fraction by less than 10 percent. For a diameter ratio of 0.75, isothermal pressure drop and maldistribution fraction decrease 38 percent and 24 percent respectively, although, thermal performance of the assembly is nearly insensitive to buoyancy-induced tube-to-fluid heat transfer enhancement and flow readjustment for both parallel and reverse flow. This is due in part to the large Peclet number tube flow, and to the values chosen for the external heating rate of the assembly and the parameters that effect radiative and convective losses from the assembly surface.

Because of the values chosen for  $\epsilon^1$ ,  $\epsilon^h$ ,  $h_a$ , and  $T_{in} + T_{dep}$ , the heat flux to the fluid is axially constant to within about 7 percent since the ratio of the rate of heat loss from the assembly surface, to the absorbed radiant flux does not increase significantly in the axial direction. Thus, the results obtained here may be applied to a corresponding plate heat exchanger where the inter-plate heat transfer rate is approximately constant.

#### ACKNOWLEDGMENT

This study was partially supported by the U. S. Department of Energy, Solar Heating and Cooling R&D Branch. One of the authors (GFJ) is also grateful for the award of the Ashton Fellowship at the University of Pennsylvania.

#### REFERENCES

- Acrivos, A., Babcock, B. D., and Pigford, R. L., 1959, "Flow Distributions in Manifolds," *Chemical Engineering Science*, 10, pp. 112-124.
- Bajura, R. A., 1971, "A Model for Flow Distribution in Manifolds," *Journal of Engineering for Power*, 93, pp. 7-12.
- Bajura, R. A., and Jones, E. H., 1976, "Flow Distribution Manifolds," *Journal of Fluids Engineering*, 98, pp. 654-666.
- Bassiouny, M. K., and Martin, H., 1984, "Flow Distribution and Pressure Drop in Plate Heat Exchangers -I," *Chemical Engineering Science*, 39, pp. 693-700.
- Bassiouny, M. K., and Martin, H., 1984, "Flow Distribution and Pressure Drop in Plate Heat Exchangers -II," *Chemical Engineering Science*, 39, pp. 701-704.
- Bliss, R. W., 1959, "The Derivation of Several 'Plate Efficiency Factors' Useful in the Design of Flat-Plate Solar-Heat Collectors," *Solar Energy*, 3, pp. 55-64.
- Chiou, J. P., 1982, "The Effect of Nonuniform Fluid Flow Distribution on the Thermal Performance of Solar Collector," *Solar Energy*, 29, pp. 487-502.
- Chiou, J. P., 1979, "Noniterative Solution of Heat Transfer Equation of Fluid Flow in Solar Collector," ASME Paper No. 79-WA/SOL-24.
- Churchill, S. W., and Ozoe, H., 1973, "Correlations for Laminar Forced Convection with Uniform Heating in Flow over Flat Plate and in Developing and Fully Developed Flow in a Tube," *Journal of Fluids Engineering*, 100, pp. 177-179.

Eno, B.. 1967. "Combined Convection and Radiation from Rectilinear Fins." Proc. ASHRAE Semi-annual Meeting, Detroit, MI.

Gupta, S. K., and Tanfi, K. K.. 1977. "Computer Program for Solution of Large Sparse Unsymmetric Systems of Linear Equations." Int. Journal for Num. Meth. in Eng. 11, pp. 1281-1289.

Hoffman, E. W., and Flannery, V. C.. 1985. "Investigation of Flow Distribution in Solar Collector Arrays." Proc. International Solar Energy Society Conference, Montreal, Canada, pp. 1008-1012.

Hottel, H. C., and Woertz, B. B., 1942. "The Performance of Flat Plate Solar-Heat Collectors." Journal of Heat Transfer, 64, pp. 91-104.

Jones, G. F., and Lior, N.. 1978. "Isothermal Flow Distribution in Solar Collectors and Collector Manifolds." Proc. American Section of the International Solar Energy Society Conference, Denver, CO, pp. 362-367.

Keller, J. D., 1949. "The Manifold Problem." Trans. ASME, 71, p. A-77.

Lawrence, W. T., and Chato, J. C., 1966. "Heat Transfer Effects on the Developing Laminar Flow Inside a Vertical Tube." Journal of Heat Transfer, 88, pp. 214-222.

Lieblein, S., 1959. "Analysis of Temperature Distribution and Radiant Heat Transfer Along a Rectangular Fin of Constant Thickness," NASA Technical Note D-196.

Manner, W. J., and McMillan, H. K., 1970. "Combined Free and Forced Laminar Convection in a Vertical Tube with Constant Wall Temperature," Journal of Heat Transfer, 92, pp. 559-562.

McNown, J. S., 1954. "Mechanics of Manifold Flow," Trans. ASCE, 119, pp. 1103-1142.

Menuchin, Y., Bassler, S., Jones, G. F., and Lior, N. 1981. "Optimal Flow Configuration in Solar Collector Arrays." Proc. American Section of the International Solar Energy Society Conference, Philadelphia, PA, pp. 616-620.

Plamondon, J. A., and Landram, C. S., 1966. "Radiant Heat Transfer from Nongray Surfaces with External Radiation." Prog. Astro. and Aero., 18, pp. 173-197.

Shah, R. K., 1978. "A Correlation for Laminar Hydrodynamic Entry Length Solutions for Circular and Noncircular Ducts," Journal of Fluids Engineering, pp. 177-179.

Sotos, C. J., and Stockman, N. O., 1964. "Radiant-Interchange View Factors and Limits of Visibility for Differential Cylindrical Surfaces with Parallel Generating Lines," NASA Technical Note D-2256.

Sparrow, E. M., and Paghri, M., 1980. "Fluid-to-Fluid Conjugate Heat Transfer for a Vertical Pipe-Internal Forced Convection and External Natural Convection," Journal of Heat Transfer, 102, pp. 402-407.

Sparrow, E. M., and Krowech, R. J., 1977. "Circumferential Variations of Bore Heat Flux and Outside Surface Temperature for a Solar Collector Tube," Journal of Heat Transfer, 99, pp. 360-366.

Whillier, A., 1953. "Solar Energy Collection and Its Utilization for House Heating," Sc.D. Thesis, M.I.T., Cambridge, MA.

Window, B., and Harding, G. L., 1983. "Buoyancy Effects and the Manifolding of Single Ended Absorber Tubes." Solar Energy, 31, pp. 153-157.

Zeldin, B., and Schmidt, F. W., 1972. "Developing Flow with Combined Forced-Free Convection in an Isothermal Vertical Tube." Journal of Heat Transfer, 94, pp. 211-223.